ISA Transactions 141 (2023) 470–481

Contents lists available at ScienceDirect

ISA Transactions

journal homepage: www.elsevier.com/locate/isatrans

Practice article

Switched step integral backstepping control for nonlinear motion systems with application to a laboratory helicopter

A. Haruna [a,b], Z. Mohamed [a,*], M.Ö. Efe [c], A.M. Abdullahi [b]

[a] Faculty of Electrical Engineering, Universiti Teknologi Malaysia, 81310 UTM Johor Bahru, Johor, Malaysia
[b] Department of Mechatronics Engineering, Bayero University Kano, Nigeria
[c] Department of Computer Engineering, Hacettepe University, Turkey

ARTICLE INFO

Article history:
Received 28 October 2021
Received in revised form 2 July 2023
Accepted 2 July 2023
Available online 4 July 2023

Keywords:
Backstepping
Energy efficiency
Nonlinear control
Switched control
Twin rotor

ABSTRACT

In this paper, the energy efficiency of the widespread application of backstepping control to a class of nonlinear motion systems is investigated. A Switched Step Integral Backstepping Control (SSIBC) scheme is introduced to improve immunity to measurement noise and to increase the energy efficiency of conventional backstepping in practice. The SSIBC is realized by switching between two candidate controllers obtained at different steps of the iterative backstepping design process. A bi-state dependent hysteresis rule is developed to supervise stable switching between the different regimes in the presence of noise. The proposed method is experimentally verified on a MIMO twin rotor laboratory helicopter involving coupled nonlinear dynamics, inaccessible states and uncertainties. Experimental results show that in addition to a reduction in power consumption, the SSIBC reduces saturation of the control signal and visible motor jerking in contrast with conventional backstepping. Additional comparisons with a previously proposed optimized decoupling PID controller also show significant improvement in precision achieved with higher energy efficiency. Experimental results obtained with the introduction of an external disturbance into the system also show the robustness of the proposed SSIBC.

1. Introduction

Owing to its recursive and systematic design methodology, the backstepping technique provides an effective method for stabilizing nonlinear systems in cascade or strict-feedback form [1]. Consequently, various backstepping control methodologies have been proposed for many rigid body nonlinear motion systems. For example, backstepping with quaternion feedback was proposed for satellite attitude control [2] and with fuzzy control for a robotic system [3]. Adaptive backstepping [4,5] and command filtered backstepping [6] were proposed for electrohydraulic systems. In [7], observer backstepping was proposed for a dynamic positioning system while adaptive backstepping, backstepping with neural networks and 2-step integral backstepping were respectfully suggested for Unmanned Aerial Vehicle (UAV) platforms in [8–10]. Although well suited to these systems (as the output state variable is of type position and the others are its derivatives i.e. velocity and acceleration), the backstepping law can, however, be quite difficult to implement in practice. One major bottleneck is that in conventional recursive backstepping, the number of required steps (iterations) equals the relative degree identifier of the system i.e. the number of times the output needs to be differentiated to explicitly arrive at the input [11]. Thus, in practical applications, noise emanating from sensory devices gets amplified after each step, leading to high harmonic content and saturation of the control signal. This can induce tracking error and undesirable mechanical vibrations as a consequence of actuator saturation [7,12–14] and also results in decreased efficiency of electrical motors [15]. Furthermore, many practical systems have inaccessible states that need to be estimated in real time via observers or other derivative estimators/filters. Thus, dealing with measurement noise becomes more problematic as there is a performance trade-off between speed/accuracy of state reconstruction and noise amplification [16].

Improving immunity to noise in backstepping as well as other state feedback control approaches has motivated extensive research work in state estimation and noise attenuation strategies. For instance, a low speed velocity estimator [17] and switched gain observers [16] have been suggested to recover system states with reduced noise in the low speed operation regions i.e. around steady state. In [7], two gain matrices associated with error variables were employed with observer backstepping to reduce amplification of noise resulting from non-perfect state estimation into the control signal. This, however, has the drawback of complicating the control law and demands tuning of additional

* Corresponding author.
E-mail address: zahar@fke.utm.my (Z. Mohamed).

https://doi.org/10.1016/j.isatra.2023.07.002
0019-0578/

parameters. Measures like filtering as proposed in [18,19] for example, have also been applied to reduce the noise profile of feedback control signals. Deployment of filters, however, must be done cautiously as they invariably introduce time lags, which can degrade system performance or even cause instability.

Other methods have been studied to avoid the calculation of noisy time derivatives. This has been proposed in [6] using command filtered backstepping for the pitch control of a wind turbine and in [20] by exploiting the flatness property of an electrohydraulic system. However, the methods in [6,20] are better suited to systems having fast actuator dynamics. Moreover, an error compensation mechanism was required in [6] to reduce the deviation introduced by the command filter. In [21], sensor-based backstepping was suggested (with the aid of an acceleration sensor) for a fixed-wing aircraft to reduce the effects of uncertainties and measurement noise. In many motion systems, however, it is not always practical or desirable to employ acceleration sensors, which are known for introducing measurement noise.

The main contribution of this work is to improve the measurement noise immunity and thereby increase the precision and energy efficiency of conventional backstepping in practical motion systems in the presence of inaccessible states and uncertainties. The proposed method, termed Switched Step Integral Backstepping Control (SSIBC), yields energy efficient and real time output regulation of relative degree 3 motion systems. Many motion control systems such as those in [2–4,6–9,22] can be considered as relative degree 3 by modelling the actuator as a first order system (see [7,12,22] for example). The proposed SSIBC design involves switching between two candidate backstepping controllers realized at different steps of the recursive design process. The novelty introduced here is the unique method in which the candidate controllers are designed using iterative backstepping and a bi-state dependent hysteresis scheme devised to appropriately supervise stable switching between the different regimes. The hysteresis switching rule is formulated to activate a full state conventional (3-step) IBC during the transient (high speed) phase and switch to a reduced order (2-step) IBC shown to have better noise immunity and higher energy efficiency during the low speed or tracking phase. The advantages of the SSIBC include:

(1) The overall control law exhibits the good transient response of conventional backstepping which does not suffer from the noise amplification problem in the high speed regions.
(2) The adverse effects of measurement noise amplification in conventional backstepping are significantly decreased in the low speed regions without the use of a denoising filter.
(3) No supplementary candidate control law has to be designed (as opposed to other supervisory control schemes) and retuning of control parameters is not required.
(4) Fast convergence to a close neighbourhood of the origin is guaranteed in the presence of noise through enforcement of slow-on-the-average switching between the stable candidate controllers.

The proposed SSIBC is experimentally verified on a laboratory UAV platform known as the Two-Rotor Aero-dynamical System (TRAS). The TRAS and similar platforms emulate complex aircraft manoeuvres [23] and present a challenging control problem. They are in many ways similar to a helicopter having complex nonlinear dynamics, cross-couplings and inaccessible states [24]. Besides, common laboratory helicopter platforms are not equipped with a rotor swashplate mechanism. As such, lift is generated by varying the rotor speeds thereby resulting in a delayed response, which further complicates the control problem.

Several control methodologies have been proposed in the literature for the TRAS and other similar 2 degree-of-freedom (DOF) helicopter test beds. In [22], four independent PID controllers tuned by a Modified method of a Real-type Genetic Algorithm (M-RGA) were proposed. Other PID-based methodologies suggested include active disturbance rejection control [23,25] and fuzzy logic based schemes [26–28]. However, with the exception of results in [22] where only simulation studies were done, none of the PID or fuzzy based methods investigate the energy efficiency of the proposed controllers. Moreover, the nonlinearities in the system are not handled explicitly and the composite input shaping method proposed in [25] is known to result in a much slower transient response.

Nonlinear algorithms such as feedback linearization [29,30] and sliding mode control (SMC) [31,32] have also been proposed to directly tackle the system's nonlinearities and improve robustness against uncertainties. In [33], backstepping control with a novel integral scheme was suggested. Simulation results therein showed improved precision with reduced control effort in comparison with the M-RGA PID in [22] and the SMC in [31]. Experimental verification of the method in [33] was provided in [12] with a one-off backstepping switching mechanism employed to reduce jerking of the tail (yaw) rotor at steady state. The one-off switching, however, implied that the system could not respond to set-point changes. In addition, with the exception of the feedback linearization methods in [29] where multiple models of the system were employed and in [30] where complex resetting of the derivative estimator was required, none of the methods proposed in the literature attempt to mitigate the effects of measurement noise on the energy efficiency of the system in real time. This paper, therefore, proposes a novel backstepping control design involving switching between two candidate backstepping controllers extracted from the iterative design procedure. The proposed SSIBC preserves the good transient characteristics of conventional backstepping and switches to a reduced order backstepping controller during steady state thereby reducing noise amplification, motor jerking and excessive power consumption. The switching between the candidate controllers is supervised by a simple bi-state law which considers the output of the system (position) as well as its derivative (velocity) augmented with hysteresis to guarantee energy efficient precision tracking in both the high and low speed regions.

The rest of the paper is organized as follows. Model description of the TRAS is given in Section 2, conventional integral backstepping design for the system is described in Section 3, the proposed SSIBC approach and switching signal are constructed in Section 4, the stability of the system is analyzed in Section 5 and experimental results are presented and discussed in Section 6.

2. Model description of the TRAS

The TRAS depicted in Fig. 1 consists of a beam with the main and tail rotors (driven by variable speed DC motors) attached perpendicularly at each end. The beam is pivoted at its base with an articulated joint that allows rotation in such a way that its ends move along the horizontal (yaw) and vertical (pitch) planes. Two adjustable counterbalance arms with attached weights are used to provide vertical damping. The aerodynamic thrusts from the rotors, which control the pitch and yaw angles (measured by digital position encoders) are produced by varying the rotation speeds (measured by tachogenerators) of the rotors. Each rotor affects both position angles resulting in a complex, nonlinear system with significant cross-couplings. The control objective is to quickly and accurately position the yaw and pitch angles of the helicopter-like system's beam (hovering) and follow a predetermined trajectory (tracking) in the presence of the coupling effects.

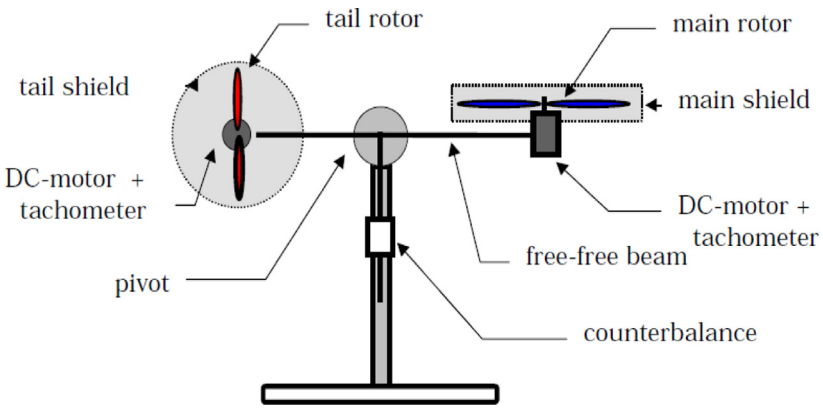

Fig. 1. TRAS components [24].

A state-space mathematical model of the TRAS is obtained from [24]. This approximate model is derived by considering the moments of inertia on each (horizontal and vertical) axis of the system using Newton's second law of motion. The derived equations describing the motion of the TRAS are given in (1).

$$\begin{aligned}
\dot{x}_1 &= x_3 \\
\dot{x}_2 &= x_4 \\
\dot{x}_3 &= \frac{1}{J_h}\left[l_t F_h(x_5)\cos x_2 - k_h x_3 + u_v k_{vh} - a_1 x_3 |x_5|\right] \\
\dot{x}_4 &= \frac{1}{J_v}\Big[\, l_m F_v(x_6) - k_v x_4 + g\left((A-B)\cos x_2 - C\sin x_2\right) \\
&\quad - \frac{1}{2}{x_3}^2 (A+B+C)\sin(2x_2)\, u_h k_{hv} + u_h k_{hv} - a_2 x_4 |x_6|\,\Big] \\
\dot{x}_5 &= \frac{1}{I_h}\left(u_h - H_h^{-1}(x_5)\right) \\
\dot{x}_6 &= \frac{1}{I_v}\left(u_v - H_v^{-1}(x_6)\right)
\end{aligned} \tag{1}$$

where x_1 (x_2) is the yaw (pitch) angle of the beam, x_3 (x_4) is the angular velocity of the beam around the horizontal (vertical) axis, u_h (u_v) is the normalized input voltage to the tail (main) rotor, x_5 (x_6) is the tail (main) rotor speed. F_h (F_v) is the propulsive force of the tail (main) rotor and ${H_h}^{-1}: x_5 \to u_h$ (${H_v}^{-1}: x_6 \to u_v$) is an inverse nonlinear function of the tail (main) rotor dynamics. The rotors are modelled as first order systems with the static nonlinearities establishing the nonlinear relationships between each motor's input voltage, rotational speed and the propulsive thrust. These nonlinear mappings are determined experimentally [24] and expressed by (2) –(5).

$$\begin{aligned}
x_5 = H_h(u_h) \approx\ & 2.2\times10^{3}{u_h}^5 - 1.7\times10^{2}{u_h}^4 - 4.5\times10^{3}{u_h}^3 \\
& + 3\times10^{2}{u_h}^2 + 9.8\times10^{3}u_h - 9.2
\end{aligned} \tag{2}$$

$$\begin{aligned}
F_h = f_h(x_5) \approx\ & -2.6\times10^{-20}{x_5}^5 + 4.1\times10^{-17}{x_5}^4 \\
& + 3.2\times10^{-12}{x_5}^3 - 7.3\times10^{-9}{x_5}^2 + 2.1\times10^{-5}x_5 + 0.0091
\end{aligned} \tag{3}$$

$$\begin{aligned}
x_6 = H_v(u_v) \approx\ & -5.2\times10^{3}{u_v}^7 - 1.1\times10^{2}{u_v}^6 + 1.1\times10^{4}{u_v}^5 \\
& + 1.3\times10^{2}{u_v}^4 - 9.2\times10^{3}{u_v}^3 - 31{u_v}^2 + 6.1\times10^{3}u_v - 4.5
\end{aligned} \tag{4}$$

$$\begin{aligned}
F_v = f_v(x_6) \approx\ & -1.8\times10^{-18}{x_6}^5 - 7.8\times10^{-16}{x_6}^4 \\
& + 4.1\times10^{-11}{x_6}^3 + 2.7\times10^{-8}{x_6}^2 + 3.5\times10^{-5}x_6 - 0.014.
\end{aligned} \tag{5}$$

Table 1 provides values of the physical parameters of the TRAS.

3. Integral backstepping control design

In this section, the controllers are designed for each subsystem of the TRAS using recursive backstepping. The system is decomposed into the horizontal subsystem (HS) and vertical subsystem (VS) so that the coupling effects form part of the system's uncertainties. The control design is similar to that in [12] and for brevity, only the main results are presented. The interested reader is referred to that article for a more detailed design.

3.1. Horizontal subsystem integral backstepping

The decomposed model of the HS can be obtained as [24]:

$$\begin{aligned}
\dot{x}_1 &= x_3 \\
\dot{x}_3 &= \frac{1}{J_h}\left[l_t F_h(x_5)\cos x_2 - k_h x_3 - a_1 x_3 |x_5|\right] \\
\dot{x}_5 &= \frac{1}{I_h}\left(u_h - H_h^{-1}(x_5)\right).
\end{aligned} \tag{6}$$

Let:

$$z_1 := x_1 - x_{1d} \tag{7}$$

$$z_3 := x_3 - \alpha_1 \tag{8}$$

$$z_5 := F_h(x_5) - \alpha_3 \tag{9}$$

where x_{1d} is the desired yaw angle and α_1 and α_3 are stabilizing functions yet to be determined.

Step 1: By considering the tracking error z_1, select a Control Lyapunov Function (CLF) candidate as:

$$V_1 = \frac{\lambda_1}{2}{\chi_1}^2 + \frac{1}{2}{z_1}^2 \tag{10}$$

where $\chi_1 = \int_0^t z_1(\tau)\, d\tau$ and λ_1 is a positive constant.

$$\alpha_1(x_1) = -c_1 z_1 - \lambda_1\chi_1 + \dot{x}_{1d},\ c_1, \lambda_1 > 0. \tag{11}$$

Step 2: Select a CLF

$$V_3 = V_1 + \frac{1}{2}{z_3}^2. \tag{12}$$

$$\dot{V}_3 = \lambda_1\chi_1\dot{\chi}_1 + z_1\dot{z}_1 + z_3\dot{z}_3. \tag{13}$$

$$\dot{z}_3 = \frac{1}{J_h}\left[l_t F_h(x_5)\cos x_2 - k_h x_3 - a_2 x_3 |x_5|\right] - \frac{\partial\alpha_1}{\partial x_1}\dot{x}_1. \tag{14}$$

$$\begin{aligned}
\dot{V}_3 = & -c_1 z_1^2 + z_3\Big[\, z_1 + \frac{l_t}{J_h}\left(F_h(x_5)\cos x_2\right) \\
& - \frac{1}{J_h}\left(k_h x_3 + a_2 x_3 |x_5|\right) - \frac{\partial\alpha_1}{\partial x_1}\dot{x}_1\,\Big].
\end{aligned} \tag{15}$$

Table 1
Physical Parameters of The TRAS [24].

Symbol	Description	Value
l_t	Length of the tail part of the beam	0.216 m
l_m	Length of the main part of the beam	0.202 m
k_h	Friction constant of the tail subsystem	5.900×10^{-2} Nm
k_v	Friction constant of the main subsystem	1.271×10^{-2} Nm
k_{vh}	Vertical angular momentum of the tail rotor	4.200×10^{-3} Nms
k_{hv}	Horizontal angular momentum of the main rotor	-1.780×10^{-2} Nms
A	Mechanical constant	0.0652
B	Mechanical constant	0.0707
C	Mechanical constant	0.0046
D	Mechanical constant	6.4608×10^{-4}
E	Mechanical constant	0.0279
F	Mechanical constant	0.0021
I_h	Moments of inertia of the tail rotor	2.703×10^{-5} kgm^2
I_v	Moments of inertia of the main rotor	1.639×10^{-4} kgm^2
a_1	Constant	9.280×10^{-6}
a_2	Constant	3.300×10^{-6}
g	Gravitational acceleration	9.810 ms^{-2}
J_v	Sum of moments of inertia relative to the horizontal axis	3.070×10^{-2} kgm^2

*The sum of moments of inertia relative to the vertical axis depends on the vertical position (x_2) of the beam and expressed as $J_h = D\sin^2 x_2 + E\cos^2 x_2 + F$.

$$\alpha_3 = \frac{J_h}{l_t \cos x_2}\left[-z_1 + \frac{1}{J_h}\left(k_h x_3 + a_2 x_3 |x_5|\right) + \frac{\partial \alpha_1}{\partial x_1}\dot{x}_1 - c_3 z_3\right]. \tag{16}$$

So that,

$$\dot{V}_3 = -c_1 {z_1}^2 - c_3 {z_3}^2, \qquad c_1, c_3 > 0. \tag{17}$$

Step 3: Select a CLF as

$$V_5 = V_3 + \frac{1}{2}{z_5}^2. \tag{18}$$

$$\dot{V}_5 = \dot{V}_1 + z_3\dot{z}_3 + z_5\dot{z}_5. \tag{19}$$

$$\dot{z}_3 = \frac{l_t \cos x_2}{J_h} z_5 - z_1 - c_3 z_3. \tag{20}$$

$$\dot{z}_5 = \frac{dF_h}{dx_5}\left(u_h - H_h^{-1}(x_5)\right) - \frac{\partial \alpha_3}{\partial x_1}\dot{x}_1 - \frac{\partial \alpha_3}{\partial x_3}\dot{x}_3. \tag{21}$$

$$\dot{V}_5 = -c_1 z_1^2 - c_3 z_3^2 + z_5\left[\frac{l_t \cos x_2}{J_h} z_3 + \frac{dF_h}{dx_5}\left(u_h - H_h^{-1}(x_5)\right) - \frac{\partial \alpha_3}{\partial x_1}\dot{x}_1 - \frac{\partial \alpha_3}{\partial x_3}\dot{x}_3\right]. \tag{22}$$

To stabilize z_5, the control input u_h is designed as:

$$u_h = H_h^{-1}(x_5) + \frac{1}{\frac{dF_h}{dx_5}}\left(-\frac{l_t \cos x_2}{J_h} z_3 + \frac{\partial \alpha_3}{\partial x_1}\dot{x}_1 + \frac{\partial \alpha_3}{\partial x_3}\dot{x}_3 - c_5 z_5\right). \tag{23}$$

So that,

$$\dot{V}_5 = -c_1 z_1^2 - c_3 z_3^2 - c_5 z_5^2 \le 0, c_1, c_3, c_5 > 0. \tag{24}$$

3.2. Vertical subsystem integral backstepping

The decomposed model for the vertical subsystem (VS) of the TRAS is obtained as [24]:

$$\begin{aligned}
\dot{x}_2 &= x_4 \\
\dot{x}_4 &= \frac{1}{J_v}\left[l_m F_v(x_6) - k_v x_4 - G(x_2) - a_2 x_4 |x_6|\right] \\
\dot{x}_6 &= \frac{1}{I_v}\left(u_v - H_v^{-1}(x_6)\right)
\end{aligned} \tag{25}$$

where $G(x_2) = g\left((A - B)\cos x_2 - C \sin x_2\right)$.

Let:

$$z_2 := x_2 - x_{2d} \tag{26}$$

$$z_4 := x_4 - \alpha_2 \tag{27}$$

$$z_6 := F_v(x_6) - \alpha_4 \tag{28}$$

where x_{2d} is the desired pitch angle and α_2 and α_4 are stabilizing functions to be obtained in the backstepping design. Using a similar design approach for the HS, the virtual control laws $\alpha_2(x_2)$ and $\alpha_4(x_2, x_4)$ for the VS are obtained as

$$\alpha_2(x_2) = -c_2 z_2 - \lambda_2 \chi_2 + \dot{x}_{2d}, c_2, \lambda_2 > 0 \tag{29}$$

where $\chi_2 = \int_0^t z_2(\tau)\, d\tau$ and λ_2 is a positive constant, and

$$\alpha_4 = \frac{J_v}{l_m}\left(-z_2 + \frac{1}{J_v}\left(G(x_2) + k_v x_4 + a_1 x_4 |x_6|\right) + \frac{\partial \alpha_2}{\partial x_2}\dot{x}_2 - c_4 z_4\right) \tag{30}$$

such that,

$$\dot{V}_4 = -c_2 {z_2}^2 - c_4 {z_4}^2, c_2, c_4 > 0. \tag{31}$$

The final control law u_v for the VS is designed as

$$u_v = H_v^{-1}(x_6) + \frac{1}{\frac{dF_v}{dx_6}}\left(-\frac{l_m}{J_v} z_4 + \frac{\partial \alpha_4}{\partial x_2}\dot{x}_2 + \frac{\partial \alpha_4}{\partial x_4}\dot{x}_4 - c_6 z_6\right) \tag{32}$$

such that,

$$\dot{V}_6 = -c_2 {z_2}^2 - c_4 {z_4}^2 - c_6 {z_6}^2 \le 0, c_2, c_4, c_6 > 0. \tag{33}$$

4. Switched step integral backstepping control (SSIBC)

In this section, the candidate controllers for each subsystem are extracted from the second and third steps of the integral backstepping design in Section 3 using output feedback. The proposed SSIBC is then realized by a bi-state dependent hysteresis switching rule to guarantee slow-on-the-average switching in the presence of noise.

4.1. SSIBC candidate controllers

The structure of the proposed SSIBC is shown in Fig. 2 where the signal $u_{h2}(u_{v2})$ is the voltage output of the 2-step IBC for the HS (VS). The blocks ${F_h}^{-1}$ (${F_v}^{-1}$) and ${x_5}^{-1}$ (${x_6}^{-1}$) represent inverse functions of the rotor static nonlinearities given in (2)–(5). These

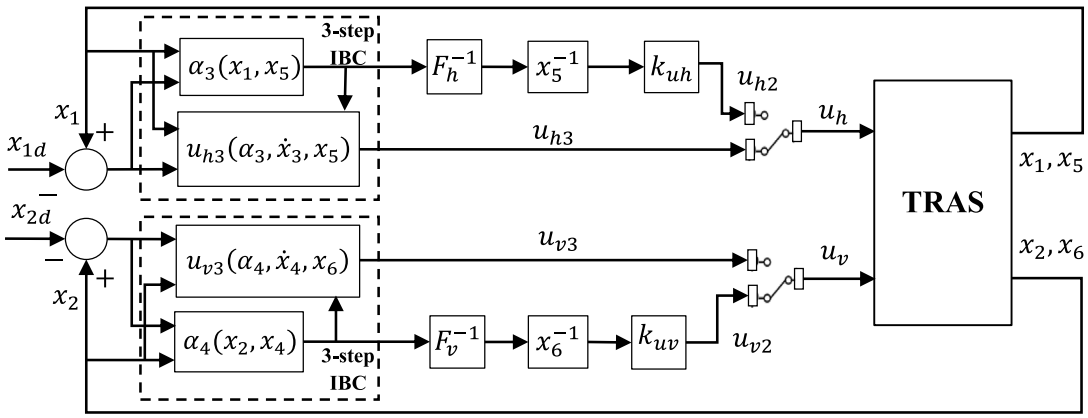

Fig. 2. TRAS SSIBC structure.

map the required force F_h (F_v) expressed by the virtual control law in (16) ((30)) into a corresponding voltage signal $u_{h2}(u_{v2})$ for the tail (main) motor. The constant gain k_{uh} (k_{uv}) is employed to achieve bumpless transfer for the HS (VS). The dashed boxes in Fig. 2 represent the conventional (3-step) integral backstepping controllers (CIBCs), which consist of the 2-step IBC and an additional (third) step of the iterative backstepping design. The 3-step CIBCs are realized after the third and final step and calculate the control outputs directly. Substituting (8) and (9) into (23) and expanding yields the 3-step CIBC control law u_{h3} for the HS as obtained in (34). Similarly, the 3-step CIBC control law u_{v3} for the VS in (35) is realized by expanding the result of substituting (27) and (28) into (32).

$$
\begin{aligned}
u_{h3} = H_h^{-1}(x_5) + \frac{1}{\frac{dF_h}{dx_5}}\{ &- \frac{l_t \cos x_2}{J_h}(x_3 + c_1 z_1 + \lambda_1 \chi_1 - \dot{x}_{1d}) \\
&- \frac{J_h}{l_t \cos x_2} x_3 [1 + \lambda_1 x_3 + c_3 (c_1 + \lambda_1 z_1)] \\
&+ \frac{J_h}{l_t \cos x_2} \dot{x}_3 \left[\frac{1}{J_h}(k_h + a_1 |x_5|) - c_1 - c_3 - \lambda_1 z_1 \right] \\
&- c_5 [F_h(x_5) - \alpha_3(x_1, x_3)] \}
\end{aligned} \tag{34}
$$

$$
\begin{aligned}
u_{v3} = H_v^{-1}(x_6) + \frac{1}{\frac{dF_v}{dx_6}}\{ &- \frac{l_m}{J_v}(x_4 + c_2 z_2 + \lambda_2 \chi_2 - \dot{x}_{2d}) \\
&- \frac{J_v}{l_m} x_4 [1 - \frac{1}{J_v}\dot{G}(x_2) \\
&+ \lambda_2 x_4 + c_4 (c_2 + \lambda_2 z_2)] \\
&+ \frac{J_v}{l_m} \dot{x}_4 \left[\frac{1}{J_v}(k_v + a_2 |x_6|) - c_2 - c_4 - \lambda_2 z_2 \right] \\
&- c_6 [F_v(x_6) - \alpha_4(x_2, x_4)] \}.
\end{aligned} \tag{35}
$$

Remark 1. The control laws for the 2-step IBCs are derived from the last terms in (34) and (35). The additional terms result from the third iteration and analytic evaluation of the partial backstepping derivatives.

Remark 2. The TRAS' beam is restricted vertically between $-\pi/2 < x_2 < \pi/2 \Rightarrow \cos x_2 > 0 \forall x_2$ in (34). Also, $H_h^{-1}(x_5)$ and $H_v^{-1}(x_6)$ are not reciprocal functions but feedforward terms representing inverse maps of the rotor static nonlinearities. Singularities in the expressions (34) and (35) that could result from $(dF_h/dx_5)^{-1}$ and $(dF_v/dx_6)^{-1}$ respectively, are checked by bounding the control inputs within the normalized input voltages of the motors. It is easy to see from (2) and (3) for the HS that $dF_h/dx_5 > 0 \forall x_5(u_h)$ for $-1 \le u_h \le 1$. Similarly, from (4) and (5), $dF_v/dx_6 > 0 \forall x_6(u_v)$ for $-1 \le u_v \le 1$. Therefore, the laws in (34) and (35) can be safely implemented in real time.

4.2. Output feedback control

Real time implementation of the derived control laws requires reconstruction of the inaccessible states of the TRAS without any delay. The 2-step IBC requires feedback of the beam velocities x_3 and x_4 while the 3-step CIBC, in addition to the beam velocities, also requires the accelerations $\dot{x}_3$ and $\dot{x}_4$. In this work, the widely used derivative filter

$$
P(s) = \frac{s}{\tau_i s + 1} \tag{36}
$$

for $i = 1, 2$ is used to provide 'estimates' of the velocities x_3 and x_4 for the HS and VS respectively. The filter (36) is neither an observer nor a velocity estimator as discussed in [34] and has been shown to preserve the asymptotic stability of the closed-loop system without placing any restrictions on the filter bandwidth [35]. The additional requirement for the acceleration of the beam for the HS (VS) $\dot{x}_3$ ($\dot{x}_4$) is then obtained via a less noisy integral scheme by solving its expression in (6) ((25)) from measurements of $x_1(x_2)$, $x_5(x_6)$ and the 'estimated' velocity of $x_3(x_4)$. This approach significantly reduces the noise propagation within the system as it avoids the reuse of the derivative filter. In fact, without this technique, the signal to noise ratio of the control signal will be low and the 3-step CIBC will be difficult to implement in real time even if an observer were used.

4.3. SSIBC switching rule

The structures of the IBC controllers in each subsystem are varied from 3 to 2-step and vice-versa by the switching signal $\sigma(t)$. A bi-state dependent hysteresis switching rule (37) based on the error and filtered velocity signals is used to determine the switching instants for the HS and VS respectively as illustrated in Fig. 3.

$$
\sigma_i(t) = \begin{cases}
2 \text{ if } & 0 \le |z_i| < \Delta_{z_i}, 0 \le |x_j| < \Delta_{x_j} \\
2 \text{ if } & \Delta_{z_i} \le |z_i| < \Delta_{z_i} + h_{z_i}, \Delta_{x_j} \le |x_j| < \Delta_{x_j} + h_{x_j}, \sigma_i = 2 \\
3 \text{ if } & \Delta_{z_i} + h_{z_i} \le |z_i| \\
3 \text{ if } & \Delta_{x_j} + h_{x_j} \le |x_j| \\
3 \text{ if } & \Delta_{z_i} \le |z_i| < \Delta_{z_i} + h_{z_i}, \Delta_{x_j} \le |x_j| < \Delta_{x_j} + h_{x_j}, \sigma_i = 3
\end{cases} \tag{37}
$$

For $i = 1, 2$ and $j = 3, 4$ where $\sigma(t) \in M = \{2, 3\}$ is a piecewise continuous switching signal and Δ_{z_i} and Δ_{x_j} are the switching thresholds, h_{z_i} and h_{x_j} are hysteresis constants to

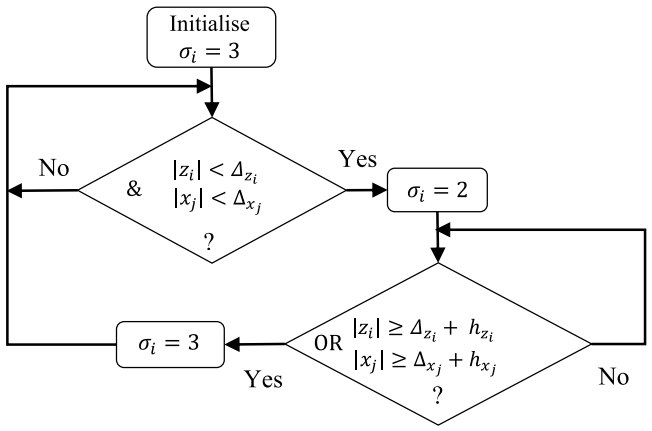

Fig. 3. SSIBC bi-state hysteresis switching logic.

prevent chattering of the switching signals [36]. The switching thresholds for the HS and VS are selected based on two theoretical and observed principles which depend on the speed region of operation of the TRAS' beam.

(1) High speed region: This region arises when the system's output is far from the reference (a transient exists) or in the case of sufficiently fast time varying reference signals which results in a high velocity of the beam. Within this region, the 3-step CIBC neither results in significant noise amplification nor excessive power consumption. Thus, the CIBC is activated when the error state z_1 (z_2) of the HS (VS) is large or when the velocity (derivative of the output) of the beam x_3 (x_4) is high.

(2) Low speed region: This region arises when the output of the system is within a close neighbourhood of the reference and has a slow rate of change (velocity). Within this region, the CIBC causes severe noise amplification as well as other undesirable effects. Thus, the 2-step IBC is activated within this boundary i.e. when both the output error z_1 (z_2) and velocity x_3 (x_4) for the HS (VS) are close to zero.

Remark 3. The switching signal $\sigma_i(t)$ can be more intuitively understood by first neglecting the hysteresis constants and assuming the system begins from rest i.e. a transient phase exits. Therefore, $|z_i| \geq \Delta_{z_i}$ which implies $\sigma_i(t) = 3$ and the 3-step CIBC is active during any transient phase. The CIBC will also be activated if the velocity of the beam exceeds its threshold i.e. $\sigma_i(t) = 3$ if $|x_j| \geq \Delta_{x_j}$. The switching signal $\sigma_i(t)$ will transition from 3 to 2 if and only if both the error (z_i) and the velocity (x_j) states fall below their respective thresholds i.e. $0 \leq |z_i| < \Delta_{z_i}$ AND $0 \leq |x_j| < \Delta_{x_j}$.

Remark 4. The hysteresis constants are added only to prevent chattering of the switching signals. That is, no transitions occur within the region containing the switching thresholds and their hysteresis constants. For instance, when $\sigma_i(t) = 3$, the CIBC remains active if $\Delta_{z_i} \leq |z_i| < \Delta_{z_i} + h_{z_i}$ OR $\Delta_{x_j} \leq |x_j| < \Delta_{x_j} + h_{x_j}$. So also when $\sigma_i(t) = 2$, the 2-step IBC remains active if $\Delta_{z_i} \leq |z_i| < \Delta_{z_i} + h_{z_i}$ AND $\Delta_{x_j} \leq |x_j| < \Delta_{x_j} + h_{x_j}$. This prevents chattering of the switching signals.

Remark 5. The signal to noise ratios of x_1 and x_2 are high and noisy estimates of x_3 and x_4 are low pass filtered in calculating the switching instants. Any delay caused by the filter does not affect performance since the filtered velocity signals are not used in calculating the control laws.

4.4. Integral action

The integral gains λ_1 and λ_2 determine the amount of integral action in (34) and (35). In the case of the undamped HS, constant integration is applied. For the VS, however, the beam is influenced by the effects of gravity and it is inherently unstable i.e. always attempting to move back to the starting (lowered) position. The gain law (38) is proposed to provide variable integral action by converging to values directly proportional to the magnitude of the initial distance between the reference and the origin. The gain law (38) enhances the tracking precision of varying setpoints for the damped VS with minimal overshoot.

$$\lambda_2 = \lambda_{2o} + k_{\lambda 2} \int |z_2|\, dt. \tag{38}$$

For $0 \leq \lambda_2 \leq \lambda_{2m}$ where $\lambda_{2m} > 0$ is the maximum integral gain, λ_{2o} is the initial integral gain for the VS and $k_{\lambda 2}$ is a positive constant determining the rate at which λ_2 reaches λ_{2m}.

5. Stability of the TRAS Under SSIBC

In this section, the stability of the TRAS with the coupling uncertainties and switching is analyzed under the proposed SSIBC.

5.1. Stability of the HS

For the decomposed HS as expressed in (6), the proposed control law u_{h3} (34) for the 3-step CIBC and u_{h2} (16) for the 2-step IBC ensure the nonpositivity of $\dot{V}_5$ in (24) and $\dot{V}_3$ in (17) respectively. Therefore, all signals are bounded and Barbalat's lemma can be invoked to show the global asymptotic stability of the origin of the decomposed HS. For the system under cross-coupled control, the cross-coupling uncertainty from the HS to the VS is given in (1) as

$$\Delta f_h = J_h^{-1}(u_v k_{vh}). \tag{39}$$

The closed-loop dynamics of the switched HS with the uncertainty in (39) can be expressed compactly in matrix form as

$$\dot{z}_h = A_{\sigma(t)} z_h + \Delta f_h \tag{40}$$

where $z_h = \begin{bmatrix} z_1 & \dots & z_{2n+1} \end{bmatrix}$ and A is an $n \times n$ skew symmetric closed-loop system matrix.

For the closed system (40), construct the Lyapunov function

$$V_{hk} = \frac{\lambda_1}{2} {\chi_1}^2 + \frac{1}{2} \sum_{j=0}^{k} z_{2j+1}^2, k \epsilon M. \tag{41}$$

The derivative of V_{hk} along the closed-loop dynamics of z_h (with the uncertainty Δf_h) is obtained as

$$\begin{aligned} \dot{V}_{hk} &= -\sum_{j=0}^{k} c_{2j+1} z_{2j+1}^2 + z_3 \Delta f_h \\ &\leq -2 \min(c_h) \frac{1}{2} z_h{}^T z_h + z_3 \Delta f_h \end{aligned} \tag{42}$$

or

$$\dot{V}_{hk} \leq -\min(c_h) \|z_h\|^2 + |z_3 \Delta f_h| \tag{43}$$

where $c_h = \begin{bmatrix} c_1 & \dots & c_{2n+1} \end{bmatrix}$.

Assumption 1. It is assumed there exists a bounded positive constant p_h such that $p_h \|z_h\|^2 \geq |z_3 \Delta f_h|, \forall t \geq 0$.

This assumption is valid as $\Delta f_h(u_v)$ is bounded for the bounded control u_v.

Assumption 2. There exist state boundaries Δ_{z_1} and Δ_{x_3} and hysteresis constants h_{z_1} and h_{x_3} such that the bi-state switching signal of the HS $\sigma_1(z_1, x_3)$ transitions on from 2 to 3 only when the states z_1 or x_3 are far away from their respective origins i.e. the system has returned to a transient state.

Assumption 2 holds since the switching thresholds can be chosen to be very close to the origin and the hysteresis constants h_{z_1} and h_{x_3} can be chosen to be sufficiently large (h_{z_1} can be taken to cover the entire operating space of the system).

Theorem 1. *If $c_h > p_h$ and Δ_{z_1}, Δ_{x_3}, h_{z_1} and h_{x_3} in (37) are chosen such that the switching signal $\sigma_1(t)$ changes from 3 to 2 according to Assumption 2, then all signals of the HS will remain globally bounded and the output will converge to a close neighbourhood of the origin for the switched control law $u_{h\sigma_1(t)}$.*

Proof. Firstly, the global asymptotic stability of the HS under the individual controllers without switching is proved and then the boundedness of all signals is shown under constrained switching.

(1) Initially, $k = 3$ and the 3-Step CIBC is active. The closed-loop dynamics of the HS in the z coordinates from (17), (20) and (21) with the uncertainty (39) can be expressed in matrix form as

$$\dot{z}_h = \begin{bmatrix} -c_1 & 1 & 0 \\ -1 & -c_3 & \frac{l_t \cos x_2}{J_h} \\ 0 & -\frac{l_t \cos x_2}{J_h} & -c_5 \end{bmatrix} z_h + \begin{bmatrix} -\lambda_1 \chi_1 \\ \Delta f_h \\ 0 \end{bmatrix} \tag{44}$$

where $z_h = \begin{bmatrix} z_1 & z_3 & z_5 \end{bmatrix}^T$. The derivative of V_{h3} along the closed-loop dynamics of z_h is obtained as

$$\dot{V}_{h3} \leq -\min(c_h) \|z_h\|^2 + |z_3 \Delta f_h| \leq 0 \tag{45}$$

where $c_h = \begin{bmatrix} c_1 & c_3 & c_5 \end{bmatrix}$. Since $\dot{V}_{h3}$ is nonpositive, it can be concluded that all signals in the z coordinates and their derivatives are bounded. It can thus be deduced from Barbalat's lemma that the closed-loop system will be globally asymptotically stable for the proposed control input $u_h = u_{h3}$ in (34). That is $\lim_{t\to\infty} z_5, z_3, z_1 \to 0$.

When $k = 2$, the 2-step IBC is active i.e. $u_h = u_{h2}, c_h = \begin{bmatrix} c_1 & c_3 \end{bmatrix}, z_h = \begin{bmatrix} z_1 & z_3 \end{bmatrix}$ and the dynamics of $\dot{z}_h$ reduces to

$$\dot{z}_h = \begin{bmatrix} -c_1 & 1 \\ -1 & -c_3 \end{bmatrix} z_h + \begin{bmatrix} -\lambda_1 \chi_1 \\ \Delta f_h \end{bmatrix} \tag{46}$$

Thus, a similar argument can be made for the 2-step IBC for z_1, z_3 and the proposed control input u_{h2} realized from (16).

(2) Consider the Lyapunov function of the closed loop switched system expressed by (41) for $k = 2, 3$. In switching from u_{h3} to u_{h2}, $V_{h3} \geq V_{h2}$ satisfies Branicky's nonincreasing condition [37] and the transition from u_{h3} to u_{h2} is stable even under arbitrary switching. When switching from u_{h2} to u_{h3}, $V_{h2} \leq V_{h3} = V_{h2} + \frac{1}{2}z_5^2$. Thus any increase in the Lyapunov function value is bounded by $\frac{1}{2}z_5^2$ which asymptotically approaches zero under the stabilizing control law u_{h3} in (34) and slow-on-the-average switching (enforced by the choices of the switching thresholds and their hysteresis constants) in accordance with Assumption 2.

Remark 6. For constant and sufficiently slowly time varying references, the switching thresholds can be chosen such that switching takes place when z_1 is in the close neighbourhood of the origin and x_3 is approximately zero i.e. the system is at steady state. Sufficiently large hysteresis constants ensure the switching stops and $\lim_{t\to\infty} z_1 = 0$.

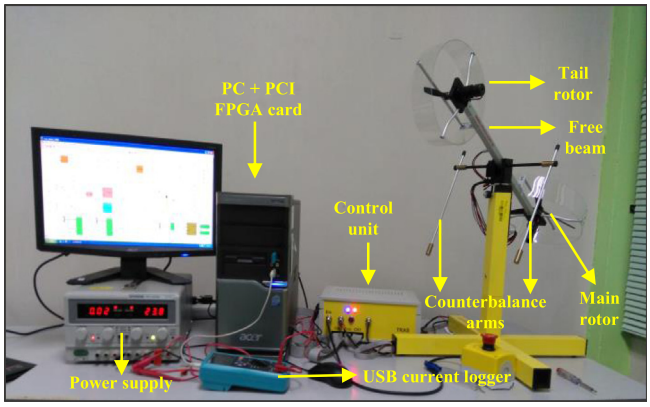

Fig. 4. TRAS experimental setup.

5.2. Stability of the VS

The TRAS' beam is physically restrained to $-\pi/2 < x_2 < \pi/2$ and the integral gain by (38) cannot change instantaneously. Applying similar arguments as in the case of the HS, the decomposed VS is thus semi-globally asymptotically stable. Under switched cross coupled control, the uncertainty in the VS from (3) is given as

$$\Delta f_v = J_v^{-1} \left(-\frac{1}{2} x_3^2 (A + B + C) \sin(2x_2) u_h k_{hv} + u_h k_{hv} \right). \tag{47}$$

Thus, similar assumptions can be made for the VS as the uncertainty $\Delta f_v(x_3, u_h)$ is bounded since x_3 (the velocity of the beam in the HS) is bounded, the decomposed HS is stable and the control input u_h is bounded. Thus, parallel arguments for the HS can be applied to establish the boundedness of all signals of the VS and the convergence of the output to within a small neighbourhood of the origin.

6. Experimental results

The designed controllers for the HS (yaw) and VS (pitch) are tested experimentally on the actual laboratory TRAS using step and sinusoidal reference inputs. The sine waves with frequency of 0.025 Hz and amplitudes of 0.5 rad and 0.2 rad are used for the HS and VS, respectively. These are similar to the reference inputs used in [22]. The laboratory setup is shown in Fig. 4 which involves the TRAS, a 24 V power supply, a control unit and a computer equipped with RT-DAC/PCI board for real time communication between the hardware and software. In this work, Matlab Real-Time Workshop software is utilized for real-time implementation of the controllers.

The transient response characteristics and integral absolute error (IAE) are used to assess the tracking performance of the controllers. The IAE is obtained by integrating the absolute difference between the output response and reference input over the experimental time (50 s) with a sampling time of 0.05 s. Meanwhile, the Rise Time (RT) is taken as the time to reach 63% of the final value, the Settling Time (ST) is computed using 95% of the final value, and the percentage Overshoot (OS) is calculated based on the maximum magnitude that exceeds the final value. The energy efficiency of controllers is determined via current measurement through an external logging device connected in series with the TRAS. This is necessary as the TRAS' motors behave like low pass filters which prohibits computing the energy efficiency of the controllers from the noisy voltage inputs. The current index (CI) is defined as the average current (milliamperes) consumption per

Table 2
Experimental control parameters.

Parameter	Value	Parameter	Value	Parameter	Value	Parameter	Value
c_1	1.05	c_6	20	τ_1	0.04	Δ_{x_4}	0.05
c_2	0.98	λ_1	0.80	τ_2	0.01	h_{z_1}	0.05
c_3	5.34	λ_2	0.81	Δ_{z_1}	0.05	h_{z_2}	0.08
c_4	11.02	λ_{2o}	0.45	Δ_{z_2}	0.02	h_{x_3}	0.1
c_5	10	$k_{\lambda 2}$	0.7	Δ_{x_3}	0.05	h_{x_4}	0.1

second of the entire TRAS system during each experiment (50 s) and is used to assess the energy efficiency of the controllers.

6.1. Experimental control parameters

For the purpose of comparison, four PID controllers are optimized on the model of the TRAS by application of the proposed fitness function and genetic algorithm (M-RGA) specifications given in [22]. The fitness function is specifically designed to simultaneously minimize the tracking error and energy cost. The optimized PID parameters for the TRAS given in [24] are used as an initial search range for M-RGA. The 2-step IBC is tuned using the same cost function as M-RGA to avoid any bias. The 3-step CIBC uses the same parameters as the 2-step IBC with the additional required parameters c_5 and c_6 heuristically tuned as a trade-off between overshoot and speed/robustness. The integral gains (λ_1, λ_2, λ_{2o} and $k_{\lambda 2}$) are selected to achieve precision tracking of the reference signal with minimal overshoot. The coefficients of the derivative filter (τ_1 and τ_2) are selected to recover the velocities of the beam x_3 and x_4 with minimal delay and noise amplification. The switching thresholds (Δ_{z_1}, Δ_{z_2}, Δ_{x_3} and Δ_{x_4}) are chosen to be as close to zero as possible. In the case of the switching hysteresis constants, the history of the systems states (z_1, z_2, x_3 and x_4) are examined under CIBC. The hysteresis constants (h_{z_1}, h_{z_2}, h_{x_3} and h_{x_4}) are then selected as the observed minimum value to prevent chattering of the switching signals. The bumpless transfer gains (k_{uh} and k_{uv}) are computed by low pass filtering and comparing the pseudo-output of the 2-step IBCs with those of 3-step CIBC. The outputs of the 2-step IBCs are then weighted by the gains $k_{uh} = 1.04$ and $k_{uv} = 1.1$ to make them approximately equal to those of the CIBC. The normalized pulse width modulated control inputs are bounded between -0.5 and $+0.5$ for the HS and between 0 and $+1$ for the VS. Values of the chosen control parameters are given in Table 2.

6.2. DOF results

To show the unique features of the 2-step, CIBC and SSIBC, the controllers are tested on the system under the same conditions in 1-DOF i.e. without the coupling effects. Fig. 5 shows the 1-DOF results obtained for the HS under the IBCs to a step reference of 1.0 rad and 1.3 rad (dotted) representing a 30% increase in the operating point. From Fig. 5, it is observed that the 2-step IBC adequately tracks the reference, but the transient response is degraded (over 20% overshoot) when the operating point is increased to 1.3 rad. In the case of the CIBC however, the output tracks the setpoint and its transient response is not affected by the shift in operating point. The better transient response of the CIBC, nonetheless, occurs at the expense of a much more noisy control signal as shown in Fig. 5. This is a well-known problem as a result of differentiation of position at a close neighbourhood of the origin i.e the low speed region. The consequence, which could be attributed to the noisy control signal, can be observed in the plots of the tail rotor speeds where that of the CIBC shows clear motor jerking not visible in the case of the 2-step IBC. The SSIBC, on the other hand, has the good transient response of the CIBC and maintains the less noise amplification and smooth response of the 2-step IBC as shown in Fig. 5.

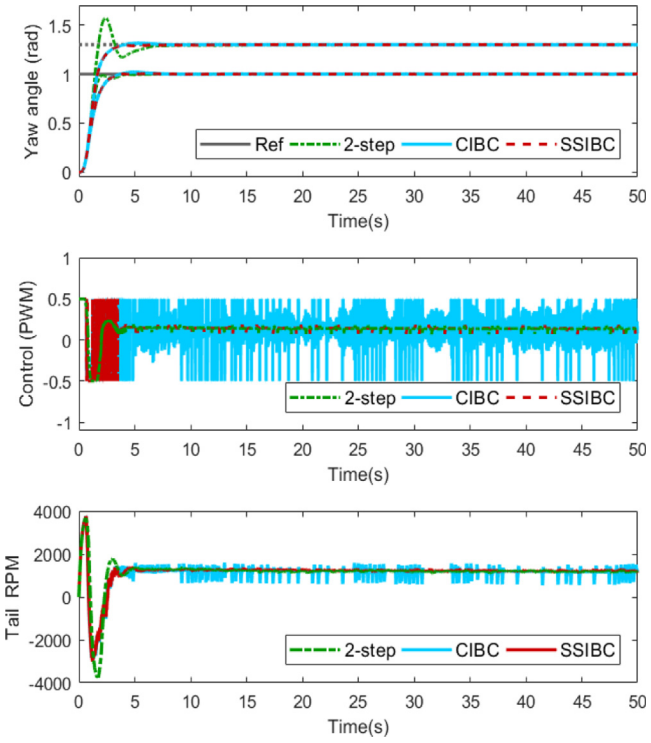

Fig. 5. 1-DOF step responses of the HS with 2-step IBC, CIBC and SSIBC.

The VS (pitch) angle responses with a sine-wave input for the IBCs also in 1-DOF are shown in Fig. 6. Again, all controllers are able to regulate the output but it is obvious that the CIBC gives a better transient response also at the cost of increased noise levels in the control signal. There is, however, no obvious effect of this on the pitch angle of the VS as the system vertically damped. In addition, the control input for the main motor is bounded between $0 \leq u_v \leq 1$. This restricts the motor from rotating in the reverse direction and prevents jerking. The response of the SSIBC is similar to that of the CIBC but with less noise amplification as shown in Fig. 6.

6.3. Cross-coupled control

Here the system is operated in 2-DOF i.e. under the high cross-coupling effects. It has already been demonstrated that the CIBC gives a better transient response than that of the 2-step. As such, for brevity, only the response under CIBC, SSIBC and M-RGA PID (for comparison) shall be considered under cross-coupled control. Fig. 7 is a step response of the system under cross-coupled control with the M-RGA PID, CIBC and SSIBC. From the output response plots in Fig. 7(a), all controllers are able to track the references and counter the cross-coupling effects. The response of the system with M-RGA PID however, shows higher overshoot and settlings times in comparison with the IBCs. The

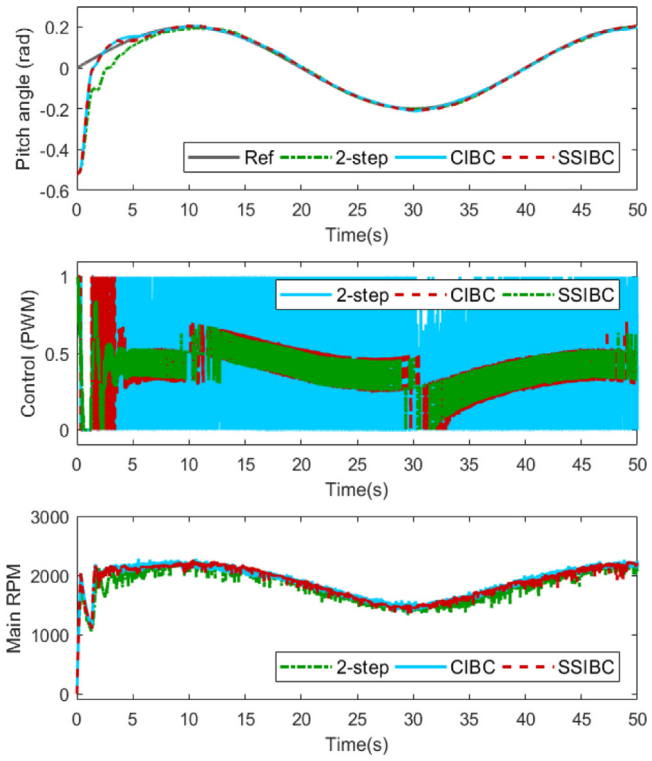

Fig. 6. 1-DOF sine responses of the VS with 2-step IBC, CIBC and SSIBC.

output plots also indicate that bumpless transfer takes place in the case of the SSIBC as its outputs seamlessly converge to the setpoints. The plot of the control signals in Fig. 7(b) both initially have high noise levels for the IBCs but that of the SSIBC show sharp decreases in the signal amplitudes at the switching instants. The effect is that jerking in the tail rotor and power consumption of the entire system are reduced.

Sine-wave tracking responses of M-RGA PID, CIBC and SSIBC are shown in Fig. 8. It is seen that all controllers achieve excellent tracking of the yaw angle. In the case of the pitch angle, however, M-RGA PID shows visible oscillations and overshoot during the transient phase. That with the CIBC also shows oscillations around the 30 s mark which do not occur under 1-DOF control shown in Fig. 6. These oscillations take place at the point where both the speed of the main rotor and velocity of the TRAS' beam are low, leading to reduced robustness of the VS and increased noise levels (from the tachometer and derivative filter). The VS is thus unable to adequately counter the cross-coupling (and jerking) effects from the tail rotor and its speed oscillates. Since the system is coupled, the HS is forced to counter this effect in order to track the yaw angle as can be seen in Fig. 8(c). These oscillations are, however, significantly minimized in the case of SSIBC due to its less noise amplification, which does not cause saturation of the control signals and jerking of the tail rotor as shown in Figs. 8(b) and 8(c). The plots of the switching signals in Fig. 8(d) indicate that the switching stops after the transient period. It can be noted with all the controllers that high peaks occur in the main and tail rotor speeds during the first 2 s approximately. This is during the transient phase for the feedback control system to achieve the desired references. Nevertheless, the global asymptotic stability of the proposed SSIBC is guaranteed by the stability analysis presented in Section 5.

Table 3 summarizes the performance of the M-RGA PID, 3-step CIBC and SSIBC in terms of their transient response, tracking and current (power) consumption characteristics. The same criteria were used in the previous research to evaluate the performance of controllers for the system [12,22,31,33]. The quantities indicate that the CIBC and the SSIBC have similar values (within experimental error) of rise time, settling time and overshoot which are much less than that of M-RGA PID. For instance, the overshoot for the IBCs is less than 7% for both the HS and VS but above 40% and 10% respectively for the HS and VS with M-RGA PID control. The IBCs also have much lower values of the IAE as compared to M-RGA PID for both the step and sine wave inputs as the values in Table 3 indicate. In the case of the step response, the CIBC and SSIBC have similar values of the IAE. For sine wave tracking, however, the SSIBC has better performance for the VS (as shown in Fig. 8) leading to a reduced value of the IAE in comparison with CIBC. Similarly, examination of the CI values in Table 3 indicate that the proposed SSIBC significantly reduces the power consumption of the entire system as compared to M-RGA PID, which in turn, consumes less energy than CIBC. The SSIBC improves the energy efficiency of conventional backstepping because it reduces the order of the backstepping control law in the low speed regions where conventional backstepping exhibits excessive energy consumption owing to noise amplification. It is worth mentioning that the computational time needed to generate the control action of SSIBC is the same as that of conventional backstepping. As the backstepping approach is an

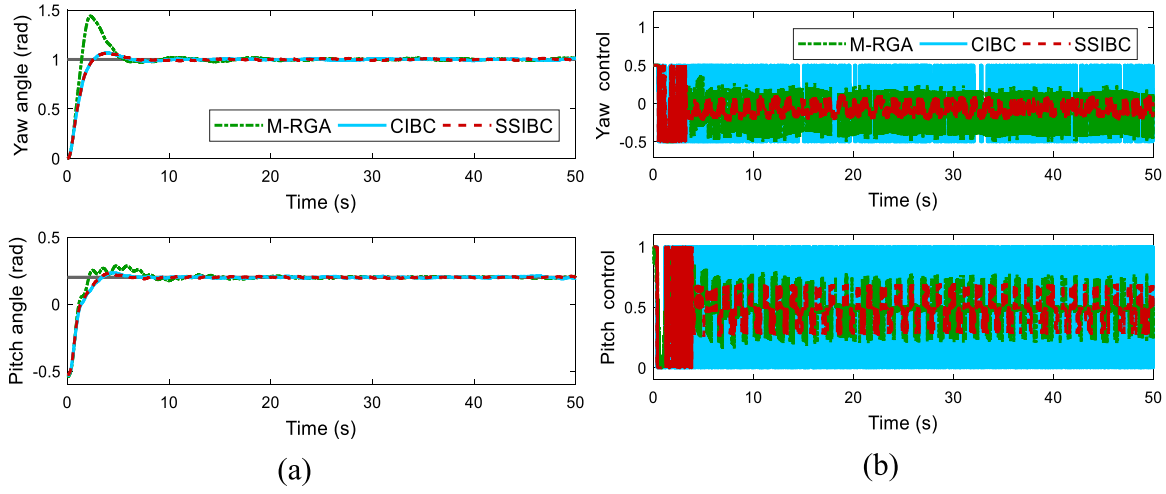

Fig. 7. Cross-coupled control for step inputs under M-RGA PID, CIBC and SSIBC: (a) Angle responses, (b) Control signals (PWM).

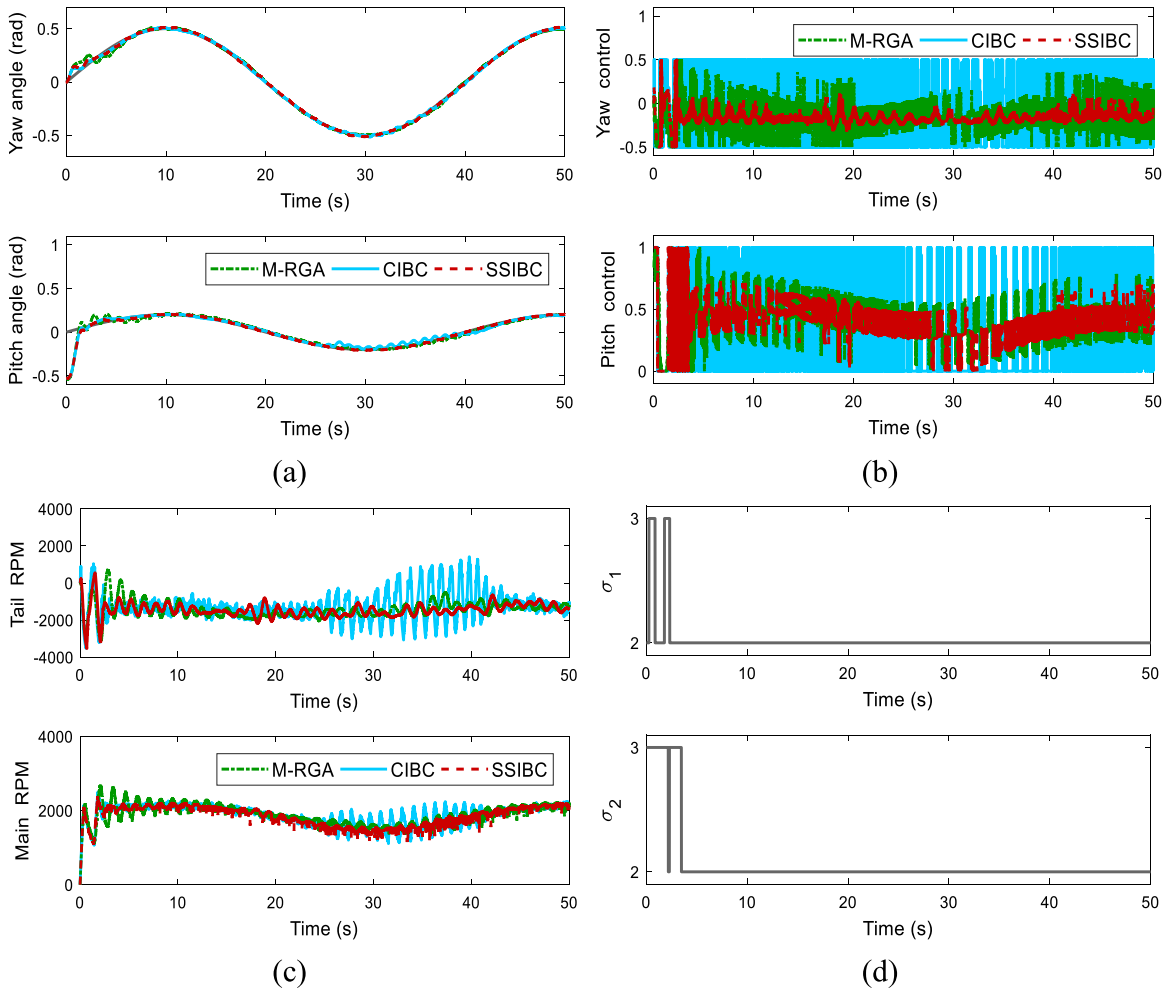

Fig. 8. Cross-coupled control for sine-wave inputs under M-RGA PID, CIBC and SSIBC: (a) Angle responses, (b) Control signals (PWM), (c) Rotor speeds, (d) SSIBC switching signals.

Table 3
Performance Characteristics of the TRAS to a Step and Sine Wave Input Under M-RGA PID, CIBC and SSIBC.

Control method	Axis	Step					Sine	
		RT (s)	ST (s)	OS (%)	IAE	CI (mA)	IAE	CI (mA)
M-RGA PID	H	1.26	4.84	43.88	42.29	628.66	12.01	525.48
	V	1.86	7.32	11.51	24.54		24.76	
CIBC	H	1.93	4.65	6.77	28.19	1012.40	7.68	1070.20
	V	2.43	2.86	4.73	21.16		22.96	
SSIBC	H	1.94	4.85	6.46	28.46	538.74	7.68	473.08
	V	2.40	2.72	4.56	19.88		15.71	

iterative design methodology, before a conventional backstepping controller (requiring 3 iterations in this case) can be designed, a 2-step controller must first be achieved. In other words, the 2-step controller is an integral part of the 3-step conventional backstepping controller.

6.4. Robustness

The robustness of the SSIBC is tested by hanging a mass of 25g attached to a peg (7g) by a string on the main part of the TRAS' beam. The angle responses obtained are shown in Fig. 9 where it is seen that the output of the VS starts from a lower position and takes a longer time to settle at the reference due to the influence of the combined 32g disturbance. At approximately 20 s, the mass is manually supported such that only the weight of the peg affects the TRAS' beam. It can be observed that the output of the VS exceeds the reference, but the controller quickly regulates the output error back to zero. At about 40 s, the mass is released, and its weight drags the pitch angle below the reference when the controller reacts again to eliminate the error. Despite that the speed of the main rotor rapidly decreases and increases to counter the effects of the disturbance, Fig. 9(a) shows that the HS is robust enough to successfully counter the cross-coupling effects by continuously tracking the yaw angle. The plot of the switching signal shown in Fig. 9(b) for the VS indicates that the SSIBC switches to the 3-step CIBC at the time instants when the disturbance is applied before switching back to the 2-step IBC after successfully countering it.

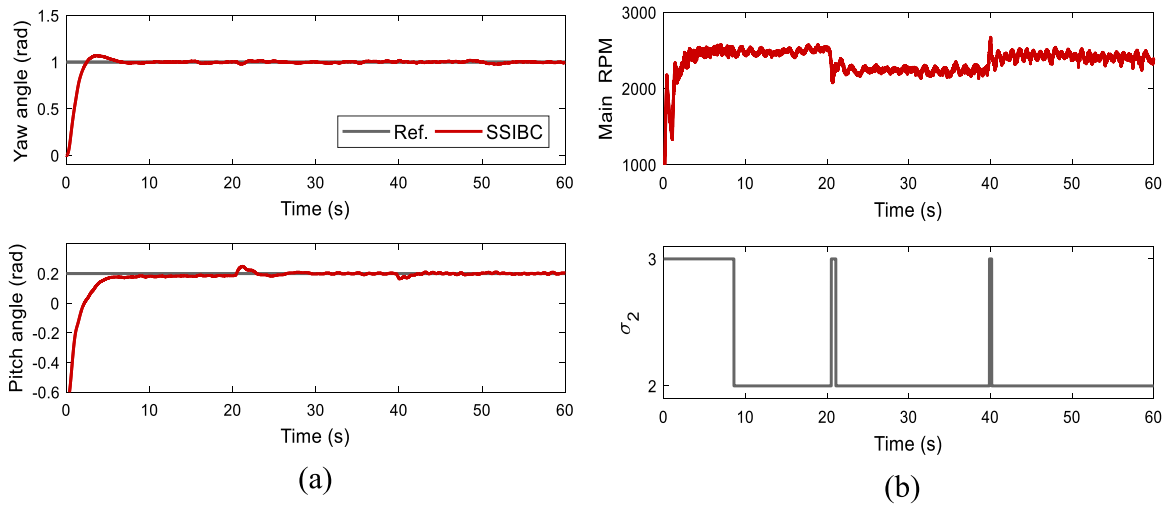

Fig. 9. Cross-coupled control of the TRAS with SSIBC subjected to an external disturbance: (a) Angle responses, (b) VS motor speed and switching signal.

7. Conclusion

A novel SSIBC algorithm has been realized by switching between two distinct candidate controllers designed after 2- and 3- steps of the iterative backstepping procedure. A developed bi-state dependent switching rule guarantees stable switching between the candidate controllers in the presence of noise and uncertainties. Experimental verification on a coupled nonlinear MIMO system has shown that the SSIBC maintains the good transient response characteristics of the conventional IBC, with less noise amplification and power consumption of the 2-step IBC during the steady/tracking phase. The experimental results also reveal that the SSIBC has much better transient and tracking characteristics achieved with reduced noise amplification and energy consumption in comparison with a previously proposed optimized decoupling (M-RGA) controller. Future work will consider a design to improve the controller robustness for the system under several types of disturbances.

Declaration of competing interest

The authors declare that they have no known competing financial interests or personal relationships that could have appeared to influence the work reported in this paper.

References

[1] Khalil HK. Nonlinear systems. Prentice Hall; 2002.
[2] Kristiansen R, Nicklasson PJ, Gravdahl JT. Satellite attitude control by quaternion-based backstepping. IEEE Trans Control Syst Technol 2009;17:227–32.
[3] Azimi MM, Koofigar HR. Adaptive fuzzy backstepping controller design for uncertain underactuated robotic systems. Nonlinear Dynam 2015;79:1457–68.
[4] Helian B, Chen Z, Yao B. Precision motion control of a Servomotor-pump direct-drive electrohydraulic system with a nonlinear pump flow mapping. IEEE Trans Ind Electron 2020;67:8638–48.
[5] Ren H, Deng G, Hou B, Wang S, Zhou G. Finite-time command filtered backstepping algorithm-based pitch angle tracking control for wind turbine hydraulic pitch systems. IEEE Access 2019;7:135514-13524.
[6] Dang X, Zhao X, Dang C, Jiang H, Wu X, Zha L. Incomplete differentiation-based improved adaptive backstepping integral sliding mode control for position control of hydraulic system. ISA Trans 2021;109:199–217.
[7] Morishita HM, Souza CES. Modified observer backstepping controller for a dynamic positioning system. Control Eng Pract 2014;33:105–14.
[8] Yang X, Zheng X. Adaptive NN backstepping control design for a 3-DOF helicopter: Theory and experiments. IEEE Trans Ind Electron 2020;67:3967–79.
[9] Haruna A, Mohamed Z, Basri M, Ramli L, Alhassan A. 2-step integral backstepping control of the two-rotor aero-dynamical system (TRAS). J Fundam Appl Sci 2017;9:395–407.
[10] Koksal N, An H, Fidan B. Backstepping-based adaptive control of a quadrotor UAV with guaranteed tracking performance. ISA Trans 2020;105:98–110.
[11] Isidori A. Nonlinear control systems. 3rd ed.. Springer Science and Business Media; 2000.
[12] Haruna A, Mohamed Z, Efe M, Basri M. Improved integral backstepping control of variable speed motion systems with application to a laboratory helicopter. ISA Trans 2020;97:1–13.
[13] Eun Y, Hamby ES. Noise induced loss of tracking in systems with saturating actuators and antiwindup. J Dyn Syst Meas Control 2014;136:DS-12-1405.
[14] Na G, Jo NH, Eun Y. Performance degradation due to measurement noise in control systems with disturbance observers and saturating actuators. J Franklin Inst B 2019;356:3922–47.
[15] Tilli A, Montanari M. A low-noise estimator of angular speed and acceleration from shaft encoder measurement. Automatika-Zagreb 2001;42:169–76.
[16] Ahrens JH, Khalil HK. High-gain observers in the presence of measurement noise: A switched-gain approach. Automatica 2009;45:936–43.
[17] Su YX, Zheng CH, Müller PC, Duan BY. A simple improved velocity estimation for low-speed regions based on position measurements only. IEEE Trans Control Syst Technol 2006;14:937–42.
[18] Merigo L, Beschi M, Padula F, Visioli A. A noise-filtering event generator for PID plus controllers. J Franklin Inst B 2018;355:774–802.
[19] Tang M, Formentini A, Odhano SA, Zanchetta P. Torque ripple reduction of PMSMs using a novel angle-based repetitive observer. IEEE Trans Ind Electron 2019;67:2689–99.
[20] Won D, Kim W, Tomizuka M. High-gain-observer-based integral sliding mode control for position tracking of electrohydraulic servo systems. IEEE/ASME Trans Mechatronics 2017;22:2695–704.
[21] Falkena W, Borst C, van Oort E, Chu Q. Sensor-based backstepping. J Guid Control Dyn 2013;36:606–10.
[22] Juang JG, Huang MT, Liu WK. PID control using presearched genetic algorithms for a MIMO system. IEEE Trans Syst Man Cybern C (Appl Rev) 2008;38:716–27.
[23] Belmonte LM, Morales R, Fernández-Caballero A, Somolinos JA. A tandem active disturbance rejection control for a laboratory helicopter with variable-speed rotors. IEEE Trans Ind Electron 2016;63:6395–406.
[24] Inteco. Two rotor aero-dynamical system user's manual inteco systems. Poland: Krakow; 2013.
[25] Yang X, Cui J, Lao D, Li D, Chen J. Input shaping enhanced active disturbance rejection control for a twin rotor multi-input multi-output system (TRMS). ISA Trans 2016;62:87–298.
[26] Singh R, Bhushan B. Adaptive neuro-fuzzy-PID and fuzzy-PID-based controller design for helicopter system. In: Applications of computing. Automation and wireless systems in lecture notes in electrical engineering, Springer; 2019, p. 281–93.
[27] Roman R-C, Precup R-E, David R-C. Second order intelligent proportional-integral fuzzy control of twin rotor aerodynamic systems. Procedia Comput Sci 2018;139:372–80.
[28] Fotuhi MJ, Bingul Z. Position and trajectory fuzzy control of a laboratory 2-DOF double dual twin rotor aerodynamical system. In: 27th IEEE international symposium on industrial electronics. 2018, p. 277–82.

[29] Pandey VK, Kar I, Mahanta C. Controller design for a class of nonlinear MIMO coupled system using multiple models and second level adaptation. ISA Trans 2017;69:256–72.
[30] Xin Y, Qin Z-C, Sun J-Q. Input–output tracking control of a 2-DOF laboratory helicopter with improved algebraic differential estimation. Mech Syst Signal Process 2019;116:843–57.
[31] Tao CW, Taur JS, Chang YH, Chang CW. A novel fuzzy-sliding and fuzzy-integral-sliding controller for the twin-rotor multi-input-multi-output system. IEEE Trans Fuzzy Syst 2010;18:893–905.
[32] Ansari U, Bajodah AH. Angular position control of twin rotor MIMO system using generalized dynamic inversion with switching surface. In: 1st international conference on unmanned vehicle systems. 2019, p. 1–6.
[33] Haruna A, Mohamed Z, Efe MÖ, Basri MAM. Dual boundary conditional integral backstepping control of a twin rotor MIMO system. J Franklin Inst 2017;354:6831–54.
[34] Loria A. Observers are unnecessary for output-feedback control of Lagrangian systems. IEEE Trans Automat Control 2016;61:905–20.
[35] Kelly R, Ortega R, Ailon A, Loria A. Global regulation of flexible joint robots using approximate differentiation. IEEE Trans Automat Control 1994;39:1222–4.
[36] Hespanha JP, Liberzon D, Morse AS. Hysteresis-based switching algorithms for supervisory control of uncertain systems. Automatica 2003;39:263–72.
[37] Branicky MS. Multiple Lyapunov functions and other analysis tools for switched and hybrid systems. IEEE Trans Automat Control 1998;43:475–82.